Journal of Neurochemistry

JOURNAL OF NEUROCHEMISTRY | 2017 | 142 (Suppl. 2) | 19–25 doi: 10.1111/jnc.13992

REVIEW

Recent developments in structural studies on acetylcholinesterase

Israel Silman* and Joel L. Sussman†

*Department of Neurobiology, Weizmann Institute of Science, Rehovot, Israel

†Department of Structural Biology, Weizmann Institute of Science, Rehovot, Israel

Abstract

This review focuses on several recent developments concerning structure–function relationships in vertebrate acetylcholinesterase. These include studies on high-resolution structures of human acetylcholinesterase and its complexes; the first crystal structure of a snake venom acetylcholinesterase, in which open and closed states of the 'back door' are visualized; a powerful algorithm for redesigning proteins for enhanced expression in prokaryotic systems, as applied to human acetylcholinesterase, which has hitherto been an intractable target; *in situ* implementation of 'click chemistry' in crystalline acetylcholinesterase, which yields novel insights into the steric and dynamic changes involved in the reaction within the active-site gorge; and a study that demonstrates the effect of crystallization conditions on ligand alignment within a protein complex, in this case the methylene blue–*Torpedo californica* acetylcholinesterase complex, which highlights the relevance of the precipitant employed to structure-based drug design.

Keywords: acetylcholinesterase, back door, click chemistry, donepezil, methylene blue, PROSS.

J. Neurochem. (2017) **142** (Suppl. 2), 19–25.

This is an article for the special issue XVth International Symposium on Cholinergic Mechanisms.

In the following, we will review some recent structural and biophysical studies on acetylcholinesterase (AChE). This will not be an attempt to provide a comprehensive review of the extensive literature on these topics, but rather will focus on a few highlights.

Structural studies on human acetylcholinesterase

The crystal structure of human AChE (hAChE) is obviously the preferred one for studies concerned with the design of drugs or of antidotes to nerve agent intoxication. That of hAChE expressed in HEK293 cells, complexed with the snake venom toxin, fasciculin-II (FAS-II), was already solved to 2.8 Å resolution (Kryger *et al.* 2000). Not surprisingly, in view of the high sequence homology of hAChE and *Tc*AChE, it overlapped very closely with that of the FAS-II–*Tc*AChE complex (Harel *et al.* 1995). A structure of native hAChE to 3.2 Å resolution (Dvir *et al.* 2010) was subsequently obtained for hAChE expressed in *Drosophila* S2 cells (Mallender *et al.* 1999). However, it is only the recent studies of Cheung and collaborators and of Nachon and collaborators that have provided high-resolution crystal structures of complexes and conjugates of hAChE, using enzyme expressed in HEK293 cells (Cheung *et al.* 2012, 2013; Beri *et al.* 2013; Franklin *et al.* 2016) or CHO-K1 cells (Nachon *et al.* 2013).

Cheung and his coworkers solved the structure of the 'non-aged' and 'aged' conjugates of hAChE with the organophosphate paraoxon to 2.15 and 2.3 Å resolution (PDB-ID 5HF5, PDB-ID 5HF6 respectively), as well as the 'non-aged' conjugate with the oxime reactivators HI-6 and 2-PAM (PDB-ID 5HF9, PDB-ID 5HFA respectively) (Franklin *et al.* 2016). They showed that phosphorylation of the active-site

Address correspondence and reprint requests to Israel Silman, Department of Neurobiology, Weizmann Institute of Science, Rehovot 76100, Israel. E-mail: Israel.silman@weizmann.ac.il; (or) Joel L. Sussman, Department of Structural Biology, Weizmann Institute of Science, Rehovot 76100, Israel. E-mail; Joel.Sussman@weizmann.ac.il

Abbreviations used: ACh, acetylcholine; AChE, acetylcholinesterase; *Bf*AChE, *Bungarus fasciatus* acetylcholinesterase; CHO, Chinese hamster ovary; *Dm*AChE, *Drosophila melanogaster* acetylcholinesterase; *Ee*AChE, *Electrophorus electricus* acetylcholinesterase; FAS-II, fasciculin-II; hAChE, human acetylcholinesterase; H-bond, hydrogen bond; HEK, human embryonic kidney; mAChE, mouse acetylcholinesterase; MB, methylene blue; OP, organophosphate; PAS, peripheral anionic site; PEG, polyethylene glycol; PROSS, Protein Repair One-Stop Shop; RMSD, root mean square deviation; *Tc*AChE, *Torpedo californica* acetylcholinesterase; wt, wild type.

serine resulted in perturbation of the acyl loop, as shown earlier for modification of *Tc*AChE (PDB-ID 2DFP) (Millard *et al.* 1999b) and mouse AChE by diisopropyl fluorophosphate (PDB-ID 2JGI for the non-aged conjugate and PDB-ID 2JGM for the aged conjugate) (Hornberg *et al.* 2007; see also recent studies by Katz *et al.* 2015). Unexpectedly, Cheung and his coworkers (Franklin *et al.* 2016) also observed that modification slightly perturbed the dimer interface, which was not described for the organophosphate conjugates of *Tc*AChE (Millard *et al.* 1999b). The structures of the ternary complexes with the oximes revealed relatively poor positioning for reactivation and valuable information for improving reactivator design.

The crystal structure to 2.35 Å resolution of the complex of donepezil (E2020) with hAChE (Cheung *et al.* 2012) revealed some differences in orientation of the bound ligand within the active-site gorge relative to the complex with *Tc*AChE (Kryger *et al.* 1999) (Fig. 1), again emphasizing the importance of the crystal structure of the human enzyme for the design of improved lead compounds based on donepezil (van Greunen *et al.* 2016).

The crystal structure of the complex with *Tc*AChE of the powerful AChE inhibitor, huprine X (Camps *et al.* 2000), which is a hybrid of tacrine and huperzine A, was earlier

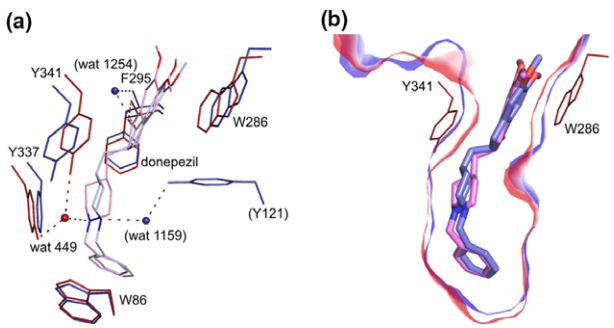

Fig. 1 Comparison of the crystal structures of the complexes of donepezil with human AChE (donepezil–hAChE; PDB-ID 4EY7) and with *Torpedo californica* AChE (donepezil–*Tc*AChE; PDB-ID 1EVE). (a) An area near the active site of the donepezil–hAChE complex is shown, with residues from *Tc*AChE superimposed. Ligand and protein atoms are shown as sticks, with waters shown as spheres. Protein residues, waters and hydrogen bonds as dash representations are colored red in the hAChE structure and blue in the *Tc*AChE structure. Nitrogen and oxygen atoms of donepezil are colored blue and red, respectively, while carbon atoms are colored pink in the hAChE complex and light blue in the *Tc*AChE complex. Residue numbering refers to hAChE, with equivalent numbers for *Tc*AChE in parentheses; (b) the superimposed active-site gorges of the complexes with donepezil of hAChE and *Tc*AChE are displayed. The red and blue 'ribbons' represent 0.5-Å-thick slices of the solvent-accessible surfaces of the hAChE and *Tc*AChE structures respectively. The bound donepezil molecules for both structures are color-coded as in (a). Residues W286 and Y341 of the human structure are shown in stick form; the equivalent *Tc*AChE residues are omitted for clarity (Kryger *et al.* 1999; Cheung *et al.* 2012).

solved to 2.1 Å resolution (Dvir *et al.* 2002). The structure of a ternary complex of hAChE with huprine W and FAS-II has now been solved to 3.1 Å resolution (Nachon *et al.* 2013). The second finger of the FAS-II does not penetrate deep enough into the gorge to interfere with the binding of the huprine. Huprine W is a potent homolog of huprine X in which the distal carbon of the ethyl substituent is hydroxylated (Ronco *et al.* 2012). The overall orientation and interactions of huprine W are similar to those described for the complexes of huprine X with *Tc*AChE (Dvir *et al.* 2002) and mouse acetylcholinesterase (mAChE) (Ronco *et al.* 2012). In particular, the tacrine-like moiety stacks against the indole of the conserved tryptophan in the 'anionic' subsite of the active site. Notably, the hydroxyl group forms strong H-bonds with the active site serine, S203, and with G122N in the oxyanion hole.

Crystal structure of *Bungarus fasciatus* AChE

Numerous scientists, including this review's authors, have made unsuccessful attempts to crystallize the monomeric form of AChE that occurs in the venom of cobras and kraits (Raba *et al.* 1979; Cousin *et al.* 1996). Crystallization, followed by solution of the structure to 2.7 Å resolution (PDB-ID 4QWW), was recently reported (Bourne *et al.* 2015) (Fig. 2). The crystals were obtained from a complex of *Bungarus fasciatus* AChE (*Bf*AChE) with an inhibitory monoclonal antibody fragment, Fab410, which was raised against *Electrophorus electricus* AChE (*Ee*AChE), and was shown, on the basis of kinetic data, to bind at the peripheral anionic site (PAS) of the enzyme at the entrance to the active-site gorge (Remy *et al.* 1995). The crystal structure confirmed the assignment made on the basis of the kinetic data. Furthermore, it revealed the coexistence of open and closed 'back door' conformations similar to those described earlier for *Drosophila melanogaster* (*Dm*) and *Torpedo californica* (*Tc*) AChE (Nachon *et al.* 2008; Sanson *et al.* 2011). The diameter of the back door was reported to be ~ 3–4 Å, a radius approximately one-half that of the constricted region located midway down the active-site gorge (Bourne *et al.* 2015).

The authors further hypothesize, on the basis of the proximity of a motif within Fab410 to residues at the exit of the back door channel, that traffic through the back door may be affected by the formation of the complex with the monoclonal antibody.

Efficient prokaryotic expression of acetylcholinesterase

Prokaryotic expression of mammalian AChE in a soluble and active form is a notoriously difficult task, which had not, in fact, been accomplished hitherto, except by refolding, in extremely poor yields, the inclusion bodies as which the

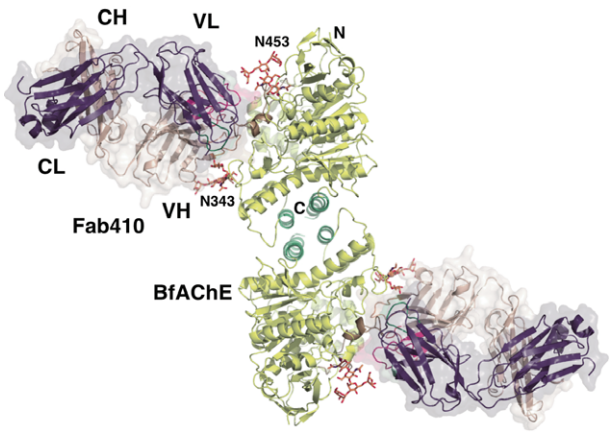

Fig. 2 Crystal structure of a complex of *Bungarus fasciatus* acetylcholinesterase with a Fab fragment (Fab410/*Bf*AChE; PDB-ID 4QWW). The figure displays both the overall structure of the complex and the electrostatic properties of the binding surfaces. Two *Bf*AChE subunits related by a two-fold symmetry axis, and linked through a tightly packed four-helix bundle composed of their $\alpha_3$7,8 and α_{10} helices, assemble as a non-covalent antiparallel dimer. Two Fab410 molecules are bound on opposite faces of the dimer, with their CDRs interacting tightly with the peripheral anionic site regions. The *Bf*AChE subunits are displayed in *yellow* with labeled N and C termini, a *green* four-helix bundle at the dimer interface, a *brown* long loop at the complex interface, *red* catalytic residues within the active-site gorges of the subunits, and *orange N*-glycan moieties linked to Asn^{343} and Asn^{453} (labeled N343 and N453 respectively). The Fab410 L and H chains and their molecular surfaces are displayed in *dark blue* and *tan*, respectively. CDRs L1, L2 and L3 are displayed in *blue*, *light green* and *dark green*, respectively, and CDRs H1, H2 and H3 are displayed in *red*, *orange* and *purple*, respectively, with H2 seen to be extended (Bourne *et al.* 2015).

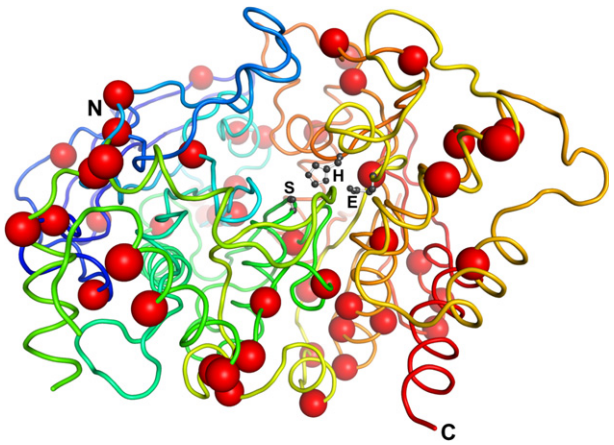

Fig. 3 Crystal structure of a designed AChE4 mutant (PDB-ID 5HQ3) generated from human AChE using the Protein Repair One-Stop Shop program. Cartoon representation of the crystal structure of human acetylcholinesterase (hAChE) displaying the mutated residues in the designed variant, dAChE4. hAChE is shown as a backbone trace, color-coded from blue at the N-terminus (labeled N) to red at the C-terminus (labeled C). The residues of the catalytic triad, Ser-203, His-447 and Glu-334 are displayed as black ball and stick models, and labeled S, H and E respectively. Fifty-one mutated residues distributed throughout the sequence are highlighted as red spheres (Goldenzweig *et al.* 2016).

protein expressed in *Escherichia coli* (Fischer *et al.* 1993; Heim *et al.* 1998). Neither molecular evolution nor computational approaches resulted in any significant success. A novel algorithm that was recently developed has now overcome this problem, and appears, in principle, to be applicable to any recalcitrant protein (Goldenzweig *et al.* 2016).

The new algorithm – which bears the acronym standing for Protein Repair One-Stop Shop – is available at http://pross.weizmann.ac.il. It scans through the entire sequence of a protein to introduce mutations that will improve such characteristics as core packing, surface polarity and backbone rigidity, at the same time excluding the introduction of deleterious mutations.

In the case of hAChE, it generated five 'design' mutants, dAChE1–dAChE5, in which 17–67 amino acid residues were mutated, corresponding to 3–12% of the total. It should be noted that mutation of residues within the active-site gorge was forbidden. All five 'design' mutants expressed well in *E. coli*, from 2 to 3 orders of magnitude better than the wild type (*wt*), yielding amounts approaching 2 mg of enzyme protein per liter of the culture. The precise enhancement in expression of soluble enzyme is hard to estimate, as *wt* expression is so poor. The kinetic constants (k_{cat} and K_m) of the designed mutants for action on acetylcholine (ACh) were very similar to those for the enzyme expressed in a *wt* eukaryotic host, but their thermal stabilities were 16–19°C higher than for the *wt*. dAChE4, which bears 51 amino acid substitutions, readily produced high-quality crystals, permitting collection of data to 2.7 Å resolution. As seen in Fig. 3, the mutations are distributed throughout the enzyme, both buried and on the surface. The overall structure of dAChE4 is very similar to that of *wt* hAChE, with an RMSD of 0.7 Å resolution for all Cα atoms. Residues in the active-site gorge align particularly well, with an all-atom RMSD of only 0.125 Å relative to the *wt*. Their active sites are thus virtually identical.

'Click chemistry' implemented *in situ* within crystalline acetylcholinesterase

The demonstration that click chemistry could be implemented efficaciously within the active-site gorge of AChE, which served as a highly selective template, opened up a fascinating avenue of research (Lewis *et al.* 2002). Specifically, this was achieved by coupling the azide and alkyne functions that participate in the Huisgen 1,3-dipolar

cycloaddition reaction – which is ideally suited to click chemistry protocols (Kolb and Sharpless 2003) – to moieties that recognize, respectively, the 'anionic' subsite of the active site and the PAS, tacrine and propidium, respectively (Manetsch *et al.* 2004), as illustrated in Fig. 4. Thus, the gorge template stereo-specifically catalyzes formation of a femtomolar *syn*-triazole inhibitor within the gorge of mAChE from a tacrine azide and a propidium alkyne, in which the length of the spacer between the ligands and the functional moieties can be varied.

Solution of the crystal structures of complexes of both the *syn*- and *anti*-triazole isomers clarified the structural basis for formation of the *syn* isomer within the gorge (Bourne *et al.* 2004). A subsequent study showed that co-crystallization with mAChE of *syn*- and *anti*-isomers of one such triazole, TZ2PA6 (in which the tacrine spacer contained two carbons and the propidium spacer six carbons), yielded, in both cases, freshly formed femtomolar complexes that, over the course of time, on a scale of days to weeks, rearranged to novel conformations of the bound ligands, which were accompanied by concerted rearrangements of amino acid side chains (Bourne *et al.* 2010).

The steric and dynamic factors that affect the course of the *in situ* cycloaddition within the active-site gorge of mAChE have now been further explored (Bourne *et al.* 2016). In this most recent study, both pairs of precursors, as well as the formed conjugates, were soaked into crystals of mAChE. The precursors taken were TZ2 and either PA5 or PA6. Soaking either PA5 or PA6 into native mAChE crystals, whether in the presence or absence of TZ2, resulted in structures devoid of ligand, as previously reported, due primarily to steric hindrance by symmetry-related mAChE molecules (Bourne *et al.* 2003). Soaking of TZ2 produced a complex in which the TZ2 bound at the 'anionic' subsite in the same pose as observed for the *anti*- and *syn*-TZ2PA5/PA6 products. It was observed, unexpectedly, that the bound ligand disrupts the catalytic triad, with H447 breaking its H-bond with E334, and swinging 180°, a rotation similar to that observed for H440 upon phosphonylation of *Tc*AChE (Millard *et al.* 1999a), except that it has no alternative partner with which to form an H-bond; such a rotation does not occur in the tacrine–*Tc*AChE complex (Harel *et al.* 1993). The rotation of H447 is accompanied by a concomitant rotation of the side chain of Y337, in turn producing high disorder in Y341, at the PAS. Thus, binding of the TZ2 precursor near the foot of the gorge appears to set in motion coordinated side-chain movements that are associated with formation of the *syn*-triazole 'click' product.

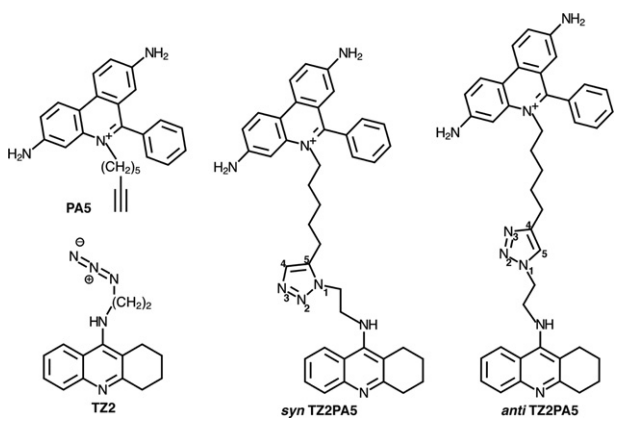

Fig. 4 Structures of the PA5 and TZ2 precursors and the *syn*- and *anti*-TZ2PA5 regioisomers formed from them by 1,3-dipolar cycloaddition. The phenyl–phenanthridinium, $4_{anti}/5_{syn}$-triazole and tacrine moieties are displayed from top to bottom (Bourne *et al.* 2016).

Attempts to soak in both TZ2 and PA5/PA6 by varying experimental conditions, such as ligand concentrations and temperature, produced crystal structures in which only TZ2 was seen, except in one data set, in which both TZ2 and PA5 were both seen, albeit with partial occupancy by PA5. In this complex, the orientation of the TZ2 is as in the TZ2–mAChE complex, and similar disruption of the catalytic triad, accompanied by rotation of H447, is observed. However, both PA5 and the residues with which it interacts undergo major conformational changes resulting both in partial occlusion of the gorge and in an orientation of the pentamethylene group bearing the alkyne moiety toward the solvent; occurrence of the *in situ* cycloaddition reaction is thus precluded. It is of interest that the orientation of the PA5 moiety resembles that of the 10-carbon alkyl chain of decidium in the decidium–mAChE complex obtained by co-crystallization, which lies on the surface rather than along the gorge axis (Bourne *et al.* 2003).

Influence of crystallization conditions on ligand alignment: implications for identification of lead compounds using docking protocols

The powerful photosensitizer methylene blue (MB) acts as a strong reversible inhibitor of *Tc*AChE in the absence of illumination, and as an irreversible inhibitor under illumination with white light (Weiner *et al.* 2011). The structure of the reversible MB–*Tc*AChE complex was later solved to 2.4 Å resolution (Paz *et al.* 2012).

It subsequently became apparent that docking of MB into the crystal structure of the complex from which the ligand had been removed produced poses that differed drastically from that of the MB in the experimental crystal structure (Wildman *et al.* 2011). The crystals used to collect data for the MB–*Tc*AChE complex had been obtained by soaking MB into crystals of native *Tc*AChE, which had been generated using polyethylene glycol 200 (PEG200) as the precipitant. Closer examination of the MB–*Tc*AChE structure revealed three PEG oligomers in the active-site gorge in the MB–*Tc*AChE complex (Dym *et al.* 2016) (Fig. 5; PDB-ID 5E4T). In particular, one such oligomer interacted with

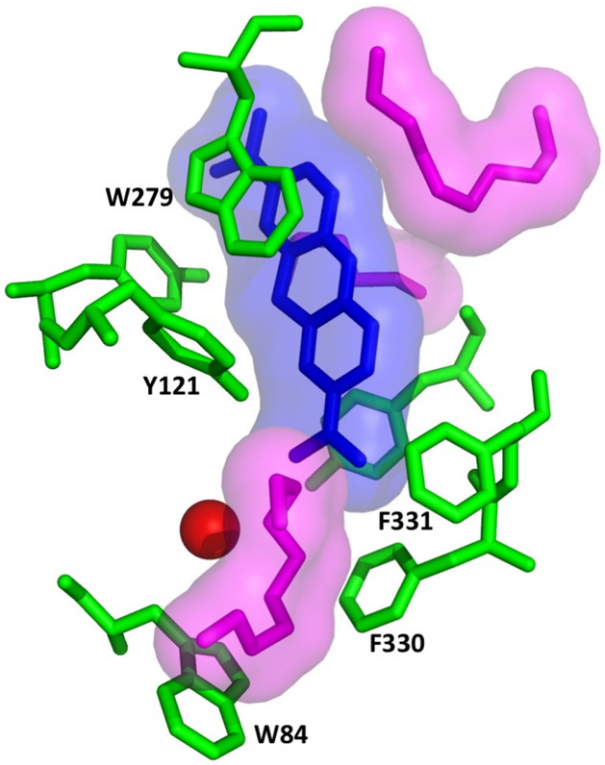

Fig. 5 Impact of ethylene glycol oligomers (polyethylene glycol, PEGs) on the positioning of the ligand in the crystal structure of the complex of methylene blue with *Torpedo californica* acetylcholinesterase [methylene blue (MB)–*Tc*AChE] obtained using PEG200 as the precipitant (PDB-ID 5E4T). PEGs are shown in magenta, MB in blue and conserved aromatic residues lining the active-site gorge in green. A highly conserved H_2O molecule, shown as a red sphere, also affects the positioning of the ligand (Dym *et al.* 2016).

W84, at the bottom of the gorge, thus preventing a π–cation interaction between the proximal nitrogen atom of MB and the indole ring of W84 similar to that often seen for complexes of *Tc*AChE with quaternary inhibitors (Harel *et al.* 1993). It is interesting that the interaction of the PEG oligomer with W84 is very similar to that earlier reported for the complex of *Tc*AChE with a thio-PEG oligomer (Koellner *et al.* 2002).

The observations described above motivated solution of the crystal structure of an MB–*Tc*AChE complex in which the crystals had been obtained using $(NH_4)_2SO_4$ as the precipitant (PDB-ID 5DLP), and thus were devoid of PEG (Dym *et al.* 2016). In this complex, the MB was positioned significantly further down the gorge, and made a π–cation interaction with W84 similar to that described for complexes of other quaternary ligands. Similar results were obtained when the structure of a decamethonium–*Tc*AChE complex obtained in the presence of $(NH_4)_2SO_4$ (Harel *et al.* 1993) was compared to that of a complex in which PEG200 served as the precipitant (Dym *et al.* 2016).

At this stage the docking data were reassessed. For this purpose, docking was performed using the XP version of Glide (Friesner *et al.* 2006), in which π–cation and π–π interactions are included in the docking algorithm. Docking was able to produce poses very similar to the experimental position of MB in both the crystal structure obtained in PEG200, and for that obtained in $(NH_4)_2SO_4$. However, in the case of the PEG200 complex, in order for an optimal pose to be achieved, it was found necessary to include, in addition to the three PEG oligomers, a conserved water molecule that had been identified earlier in five *Tc*AChE structures (Koellner *et al.* 2000).

These crystallographic observations permitted the interpretation of mass spectroscopy (MS) data, which showed that MB-induced photoxidation of *Tc*AChE to *N*-formylkynurenine oxidized almost exclusively the conserved Trp residues, W84, near the bottom of the gorge, and W279, near the top (Triquigneaux *et al.* 2012). W233, which was at almost the same distance from MB in the MB–*Tc*AChE complex obtained in the presence of PEG200, was hardly affected. However, the data subsequently collected for the complex obtained by precipitation with $(NH_4)_2SO_4$ suggest that in solution the MB within the active-site gorge is in close contact with both W84 and W279, significantly closer than W233, thus rationalizing the MS data.

Finally, we wish to stress the importance of these observations for employment of docking protocols in searching for lead compounds for drug development. It turns out that *ca.* 57% of crystal structures deposited in the Protein Data Bank were obtained using PEG as the precipitant. Yet, only in *ca.* 6% of these structures are PEG oligomers identified and assigned (Dym *et al.* 2016). Thus, docking protocols that utilize the 'naked' protein structure as the template run the risk of making seriously incorrect predictions.

Acknowledgements and conflict of interest disclosure

There are no funding sources to report for this Review. Israel Silman is the Guest Editor for the special issue "XVth International Symposium on Cholinergic Mechanisms". The other author has no conflicts of interest to declare.

References

Beri V., Wildman S. A., Shiomi K., Al-Rashid Z. F., Cheung J. and Rosenberry T. L. (2013) The natural product dihydrotanshinone I provides a prototype for uncharged inhibitors that bind specifically to the acetylcholinesterase peripheral site with nanomolar affinity. *Biochemistry* **52**, 7486–7499.

Bourne Y., Taylor P., Radic Z. and Marchot P. (2003) Structural insights into ligand interactions at the acetylcholinesterase peripheral anionic site. *EMBO J.* **22**, 1–12.

Bourne Y., Kolb H. C., Radić Z., Sharpless K. B., Taylor P. and Marchot P. (2004) Freeze-frame inhibitor captures acetylcholinesterase in a unique conformation. *Proc. Natl. Acad. Sci. USA* **101**, 1449–1454.

Bourne Y., Radic Z., Taylor P. and Marchot P. (2010) Conformational remodeling of femtomolar inhibitor-acetylcholinesterase complexes in the crystalline state. *J. Am. Chem. Soc.* **132**, 18292–18300.

Bourne Y., Renault L. and Marchot P. (2015) Crystal structure of snake venom acetylcholinesterase in complex with inhibitory antibody fragment Fab410 bound at the peripheral site: evidence for open and closed states of a backdoor channel. *J. Biol. Chem.* **290**, 1522–1535.

Bourne Y., Sharpless K. B., Taylor P. and Marchot P. (2016) Steric and dynamic parameters influencing in situ cycloadditions to form triazole inhibitors with crystalline acetylcholinesterase. *J. Am. Chem. Soc.* **138**, 1611–1621.

Camps P., Cusack B., Mallender W. D., Achab R. E., Morral J., Munoz-Torrero D. and Rosenberry T. L. (2000) Huprine X is a novel high-affinity inhibitor of acetylcholinesterase that is of interest for treatment of Alzheimer's disease. *Mol. Pharmacol.* **57**, 409–417.

Cheung J., Rudolph M. J., Burshteyn F., Cassidy M. S., Gary E. N., Love J., Franklin M. C. and Height J. J. (2012) Structures of human acetylcholinesterase in complex with pharmacologically important ligands. *J. Med. Chem.* **55**, 10282–10286.

Cheung J., Gary E. N., Shiomi K. and Rosenberry T. L. (2013) Structures of human acetylcholinesterase bound to dihydrotanshinone I and territrem B show peripheral site flexibility. *ACS Med. Chem. Lett.* **4**, 1091–1096.

Cousin X., Créminon C., Grassi J., Meflah K., Cornu G., Saliou B., Bon S., Massoulié J. and Bon C. (1996) Acetylcholinesterase from *Bungarus* venom: a monomeric species. *FEBS Lett.* **387**, 196–200.

Dvir H., Wong D. M., Harel M. *et al.* (2002) 3D structure of *Torpedo californica* acetylcholinesterase complexed with huprine X at 2.1 Å resolution: kinetic and molecular dynamic correlates. *Biochemistry* **41**, 2970–2981.

Dvir H., Silman I., Harel M., Rosenberry T. L. and Sussman J. L. (2010) Acetylcholinesterase: from 3D structure to function. *Chem. Biol. Interact.* **187**, 10–22.

Dym O., Song W., Felder C. *et al.* (2016) The impact of crystallization conditions on structure-based drug design: A case study on the methylene blue/acetylcholinesterase complex. *Protein Sci.* **25**, 1096–1114.

Fischer M., Ittah A., Leifer I. and Gorecki M. (1993) Expression and reconstitution of biologically active human acetylcholinesterase from *Escherichia coli*. *Cell. Mol. Neurobiol.* **13**, 25–38.

Franklin M. C., Rudolph M. J., Ginter C., Cassidy M. S. and Cheung J. (2016) Structures of paraoxon-inhibited human acetylcholinesterase reveal perturbations of the acyl loop and the dimer interface. *Proteins* **84**, 1246–1256.

Friesner R. A., Murphy R. B., Repasky M. P., Frye L. L., Greenwood J. R., Halgren T. A., Sanschagrin P. C. and Mainz D. T. (2006) Extra precision glide: docking and scoring incorporating a model of hydrophobic enclosure for protein-ligand complexes. *J. Med. Chem.* **49**, 6177–6196.

Goldenzweig A., Goldsmith M., Hill S. E. *et al.* (2016) Automated structure- and sequence-based design of proteins for high bacterial expression and stability. *Mol. Cell* **63**, 337–346.

van Greunen D. G., Cordier W., Nell M., van der Westhuyzen C., Steenkamp V., Panayides J. L. and Riley D. L. (2016) Targeting Alzheimer's disease by investigating previously unexplored chemical space surrounding the cholinesterase inhibitor donepezil. *Eur. J. Med. Chem.* **127**, 677–690.

Harel M., Schalk I., Ehret-Sabatier L., Bouet F., Goeldner M., Hirth C., Axelsen P., Silman I. and Sussman J. L. (1993) Quaternary ligand binding to aromatic residues in the active-site gorge of acetylcholinesterase. *Proc. Natl Acad. Sci. USA* **90**, 9031–9035.

Harel M., Kleywegt G. J., Ravelli R. B. G., Silman I. and Sussman J. L. (1995) Crystal structure of an acetylcholinesterase-fasciculin complex: interaction of a three-fingered toxin from snake venom with its target. *Structure* **3**, 1355–1366.

Heim J., Schmidt-Dannert C., Atomi H. and Schmid R. D. (1998) Functional expression of a mammalian acetylcholinesterase in *Pichia pastoris*: comparison to acetylcholinesterase, expressed and reconstituted from *Escherichia coli*. *Biochim. Biophys. Acta* **1396**, 306–319.

Hornberg A., Tunemalm A. K. and Ekstrom F. (2007) Crystal structures of acetylcholinesterase in complex with organophosphorus compounds suggest that the acyl pocket modulates the aging reaction by precluding the formation of the trigonal bipyramidal transition state. *Biochemistry* **46**, 4815–4825.

Katz F. S., Pecic S., Tran T. H. *et al.* (2015) Discovery of new classes of compounds that reactivate acetylcholinesterase inhibited by organophosphates. *ChemBioChem* **16**, 2205–2215.

Koellner G., Kryger G., Millard C. B., Silman I., Sussman J. L. and Steiner T. (2000) Active-site gorge and buried water molecules in crystal structures of acetylcholinesterase from *Torpedo californica*. *J. Mol. Biol.* **296**, 713–735.

Koellner G., Steiner T., Millard C. B., Silman I. and Sussman J. L. (2002) A neutral molecule in a cation-binding site: specific binding of a PEG-SH to acetylcholinesterase from *Torpedo californica*. *J. Mol. Biol.* **320**, 721–725.

Kolb H. C. and Sharpless K. B. (2003) The growing impact of click chemistry on drug discovery. *Drug Discov. Today* **8**, 1128–1137.

Kryger G., Silman I. and Sussman J. L. (1999) Structure of acetylcholinesterase complexed with E2020 (Aricept®): implications for the design of new anti-Alzheimer drugs. *Structure* **7**, 297–307.

Kryger G., Harel M., Giles K. *et al.* (2000) Structures of recombinant native and E202Q mutant human acetylcholinesterase complexed with the snake-venom toxin fasciculin-II. *Acta Crystallogr. Sect. D: Biol. Crystallogr.* **56**, 1385–1394.

Lewis W. G., Green L. G., Grynszpan F., Radic Z., Carlier P. R., Taylor P., Finn M. G. and Sharpless K. B. (2002) Click chemistry in situ: acetylcholinesterase as a reaction vessel for the selective assembly of a femtomolar inhibitor from an array of building blocks. *Angew. Chem. Int. Ed. Engl.* **41**, 1053–1057.

Mallender W. D., Szegletes T. and Rosenberry T. L. (1999) Organophosphorylation of acetylcholinesterase in the presence of peripheral site ligands. Distinct effects of propidium and fasciculin. *J. Biol. Chem.* **274**, 8491–8499.

Manetsch R., Krasinski A., Radic Z., Raushel J., Taylor P., Sharpless K. B. and Kolb H. C. (2004) In situ click chemistry: enzyme inhibitors made to their own specifications. *J. Am. Chem. Soc.* **126**, 12809–12818.

Millard C. B., Koellner G., Ordentlich A., Shafferman A., Silman I. and Sussman J. L. (1999a) Reaction products of acetylcholinesterase and VX reveal a mobile histidine in the catalytic triad. *J. Am. Chem. Soc.* **121**, 9883–9884.

Millard C. B., Kryger G., Ordentlich A. *et al.* (1999b) Crystal structures of aged phosphonylated acetylcholinesterase: nerve agent reaction products at the atomic level. *Biochemistry* **38**, 7032–7039.

Nachon F., Stojan J. and Fournier D. (2008) Insights into substrate and product traffic in the *Drosophila melanogaster* acetylcholinesterase active site gorge by enlarging a back channel. *FEBS J.* **275**, 2659–2664.

Nachon F., Carletti E., Ronco C., Trovaslet M., Nicolet Y., Jean L. and Renard P. Y. (2013) Crystal structures of human cholinesterases in complex with huprine W and tacrine: elements of specificity for

anti-Alzheimer's drugs targeting acetyl- and butyryl-cholinesterase. *Biochem. J.* **453**, 393–399.

Paz A., Roth E., Ashani Y., Xu Y., Shnyrov V. L., Sussman J. L., Silman I. and Weiner L. (2012) Structural and functional characterization of the interaction of the photosensitizing probe methylene blue with *Torpedo californica* acetylcholinesterase. *Protein Sci.* **21**, 1138–1152.

Raba R., Aaviksaar A., Raba M. and Siigur J. (1979) Cobra venom acetylcholinesterase. Purification and molecular properties. *Eur. J. Biochem.* **96**, 151–158.

Remy M. H., Frobert Y. and Grassi J. (1995) Characterization of monoclonal antibodies that strongly inhibit *Electrophorus electricus* acetylcholinesterase. *Eur. J. Biochem.* **231**, 651–658.

Ronco C., Carletti E., Colletier J. P., Weik M., Nachon F., Jean L. and Renard P. Y. (2012) Huprine derivatives as sub-nanomolar human acetylcholinesterase inhibitors: from rational design to validation by X-ray crystallography. *ChemMedChem* **7**, 400–405.

Sanson B., Colletier J. P., Xu Y., Lang P. T., Jiang H., Silman I., Sussman J. L. and Weik M. (2011) Backdoor opening mechanism in acetylcholinesterase based on X-ray crystallography and MD simulations. *Protein Sci.* **20**, 1114–1118.

Triquigneaux M. M., Ehrenshaft M., Roth E., Silman I., Ashani Y., Mason R. P., Weiner L. and Deterding L. J. (2012) Targeted oxidation of *Torpedo californica* acetylcholinesterase by singlet oxygen: identification of *N*-formylkynurenine tryptophan derivatives within the active-site gorge of its complex with the photosensitizer methylene blue. *Biochem. J.* **448**, 83–91.

Weiner L., Roth E. and Silman I. (2011) Targeted oxidation of *Torpedo californica* acetylcholinesterase by singlet oxygen. *Photochem. Photobiol.* **87**, 308–316.

Wildman S. A., Zheng X., Sept D., Auletta J. T., Rosenberry T. L. and Marshall G. R. (2011) Drug-like leads for steric discrimination between substrate and inhibitors of human acetylcholinesterase. *Chem. Biol. Drug Des.* **78**, 495–504.